TELKOMNIKA Telecommunication, Computing, Electronics and Control
Vol. 19, No. 5, October 2021, pp. 1648~1653
ISSN: 1693-6930, accredited First Grade by Kemenristekdikti, Decree No: 21/E/KPT/2018
DOI: 10.12928/TELKOMNIKA.v19i5.20484

Integrating SiO_2 nanoparticles to achieve color uniformity and luminous efficiency enhancement for white light emitting diodes

Phan Xuan Le[1], Phung Ton That[2]
[1]Faculty of Engineering, Van Lang University, Ho Chi Minh City, Vietnam
[2]Faculty of Electronics Technology, Industrial University of Ho Chi Minh City, Vietnam

Article Info

Article history:

Received Sep 9, 2020
Revised Aug 23, 2021
Accepted Aug 31, 2021

Keywords:

Color uniformity
Luminous flux
Mie-scattering theory
SiO_2

ABSTRACT

A phosphor structure with SiO_2 nanoparticles is proposed to achieve the enhancement in the correlated color temperature (CCT) homogeneity and the luminescence performance for white light-emitting diodes (WLEDs). As SiO_2 is integrated into the phosphorus compound, the scattering effect of this material contributes to better blue-light utilization. Thus, this innovative packaging design results in a significant increased lumen efficiency, more than 12%, in comparison with that of conventional dispensing ones. Meanwhile, the angular CCT deviation also decreases considerably, from 522 K to 7 K, between the angles of -70 and 70^0. Moreover, this reduction leads to the diminishment of yellow ring phenomenon effect. In addition, the measurement of haze demonstrates that there is a strong scattering in the visible spectrum when SiO_2 is added into the silicone film. Besides that, when increasing the driving current, SiO_2 stabilizes the chromaticity coordinate shift, which is a vital requirement for indoor lighting applications. Furthermore, SiO_2 nanoparticles own excellent optical features, cost efficiency, and simple production will probably turn this material into a potential material in advancing the optical performance of WLEDs.

Corresponding Author:

Phung Ton That
Faculty of Electronics Technology
Industrial University of Ho Chi Minh City
No. 12 Nguyen Van Bao Street, Ho Chi Minh City, Vietnam
Email: tonthatphung@iuh.edu.vn

1. INTRODUCTION

In modern lighting applications market, light-emitting diodes (LEDs) have risen quickly as a potential and effective solid-state lighting source, which is on account of their cost efficiency, long lifespan, environmental friendliness, and higher durability [1]-[5]. LEDs are applied for both outdoor and indoor lightings, for example, street lighting, billboard lighting, museum and display lightings [5]-[8]. Especially, when it comes to indoor illumination aspect, traditional light bulbs applications have been reduced significantly as LEDs have taken over [9]. The packaging design that has been widely used for LED fabrication is structured from the combination of blue LED chips and a yellow phosphor ($Y_3Al_5O_{12}:Ce^{3+}$ or YAG) layer. However, the color rendering index (CRI) quality from this method is very low, which leads to the concern of advancing the packaging structure of LEDs to get better optical outcomes [10]-[12]. In order to address the problem of low CRI, researchers introduced several advanced structures regarding the integration of red phosphor particles into the package. Besides that, structures with multiple lateral quantum wells (QWs) and facets that yielded various emission spectra and enhanced the white light quality for LED devices have also been mentioned [13]-[15]. Researchers also have come up with techniques that can minimize the charge separation in InGaN QWs, for instance, large overlap QWs and the surface plasmon, for achieving the improvement of the IQE in green/yellow/red spectral zones; and such enhancements are crucial to the quality of the tricolor InGaN QW LEDs. When it comes to cost-saving and simple white light-emitting diode (WLED) fabrication, freely dispensing technique is the most suitable one [16]. However, the lumen output and the correlated color temperature (CCT) homogeneity of this method require significant developments to match demands from advanced lighting applications [17]. The solution for a better lumen efficacy is to increase light extraction efficiency, or in other words, increase the amount of photons going through the phosphor layers in the LED packages. Many methods aiming to the light extraction improvement have been introduced and experimented, and one of them is the dual-encapsulation layer structure which arranges the phosphor layers based on their refractive index (RI). Besides that, the phosphor-on-top design was utilized by Luo's group to advance the phosphor performance. Based on the concept of remote phosphor packaging, the phosphor layer was appropriately separated from the blue LED chips to avoid the backscattering effect to occur to emitted light from phosphor particles [18]-[22]. Together with luminous efficacy, chromatic homogeneity greatly contributes to the quality of WLEDs. Thus, enhancing the color uniformity is one of the major concerns in WLED production. A previous research pointed out the cause of this problem is the unequal proportion between the emissions of blue and yellow lights, which leads to the non-uniformity of the angular CCT. From this, the yellow ring phenomenon that causes a discomfort to human eyes occurs [23], [24]. Therefore, it is essential to eliminate such negative impact on LED devices, especially in large-scale applications. In an attempt to reduce the CCT deviation, solutions including remote phosphor design, applied by Kuo et al., conformal-phosphor structure, advanced silicone lens, and shape modification for the surface of phosphor layers in LED packages were demonstrated. Besides these methods, patterned sapphire substrate was applied to optimize the LED packaging structure to achieve the homogenous angular CCT. Researchers also reported the efficiency of the graded-refractive-index multi- encapsulation layer configuration by getting nanoparticles integrated into the packaging materials. As a result, the optical path in the package is affected due to the strong scattering effect of these nanoparticles, causing the CCT deviation to change at different angles. Though this structure could enhance the color uniformity, it results in low luminous efficiency [25]-[27]. Hence, having a structure that can give enhancement to both lumen output and chromatic homogeneity simultaneously is still a difficult but provocative question for researchers. This study incorporates SiO_2 into the phosphor layer to simultaneously achieve high lumen efficacy and CCT uniformity for WLED packages. With the presence of SiO_2 nanoparticles, the scattering effect of phosphor package is enhanced, which activates the advanced blue-light utilization. Thus, the lumen output is improved significantly. At the same time, this enhancement in scattering ability by SiO_2 reduces the angular CCT deviations, leading to a better color homogeneity.

2. SIMULATION AND COMPUTATION

2.1 MC-WLED simulation

In the traditional package, the encapsulation layer contains only two materials: the silicone and the yellow phosphor which are mixed uniformly. To integrate SiO_2 nanoparticles into the packaging of WLEDs, the dispensing technique was modified (moretech precision technology). Figure 1 shows an actual WLED and the schematic diagram simulated SiO_2-doped WLED model. The experimented model was fabricated by initially attached a GaN-based blue chip having 50 nm emission wavelength to the lead frame; and then SiO_2 nanoparticles are evenly blended together with YAG yellow phosphor (Intematix) and the silicone. After that, this mixed encapsulation layer is dispensed in the package. The full width at half maximum (FWHM) of YAG phosphor emission is about 100 nm. The used blue chip has an output power of 120 mW at 120 mA driving current. Additionally, SiO_2 particles are added into the encapsulant with various weight percentages to analyze how SiO_2 affect the performance of lumen output and CCT uniformity. The diameter of YAG and SiO_2 particles are set at around 10 mm and 300 nm, respectively.

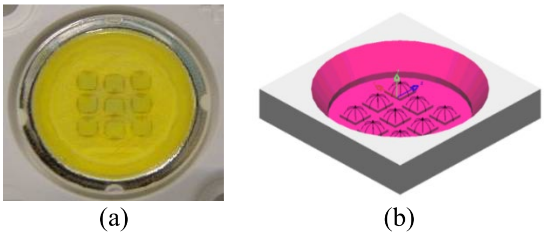

(a) (b)

Figure 1. (a) Photograph of a WLED sample, (b) The simulated WLED model

2.2. Scattering computation

The computation of scattering coefficient $\mu_{sca}(\lambda)$, anisotropy factor $g(\lambda)$, and reduced scattering coefficient $\delta_{sca}(\lambda)$ based on the Mie theory is expressed as [25]-[27]:

$$\mu_{sca}(\lambda) = \int N(r) C_{sca}(\lambda, r) dr \quad (1)$$

$$g(\lambda) = 2\pi \int \int_{-1}^{1} p(\theta, \lambda, r) f(r) \cos\theta d\cos\theta dr \quad (2)$$

$$\delta_{sca} = \mu_{sca}(1 - g) \quad (3)$$

In which, $N(r)$ indicates the distribution density of diffusional particles (mm^3), C_{sca} means the scattering cross sections (mm^2), λ is the symbol of light wavelength (nm), r is the diameter of diffusional particles (μm), $p(\theta,\lambda,r)$ presents the phase function, θ is the scattering angle (°C), and $f(r)$ represents the size distribution function of the diffusor in the phosphor layer. In addition, $f(r)$ is computed by:

$$f(r) = f_{dif}(r) + f_{phos}(r) \quad (4)$$

$$\begin{aligned} N(r) &= N_{dif}(r) + N_{phos}(r) \\ &= K_N . [f_{dif}(r) + f_{phos}(r)] \end{aligned} \quad (5)$$

As can be seen in (5), $N(r)$ is comprised of $N_{dif}(r)$ and $N_{phos}(r)$, both of which are the diffusive particle density and the phosphor particle density, respectively. $f_{dif}(r)$ and $f_{phos}(r)$ indicate the size distribution function data of the diffusor and phosphor particle, while K_N shows the number of the diffusor unit for one diffusor concentration and can be computed by:

$$c = K_N \int M(r) dr \quad (6)$$

Here, $M(r)$ indicates the mass distribution of the diffusive particles, demonstrated as:

$$M(r) = \frac{4}{3}\pi r^3 [\rho_{dif} f_{dif}(r) + \rho_{phos} f_{phos}(r)] \quad (7)$$

with $\rho_{diff}(r)$ and $\rho_{phos}(r)$ are the density of diffusor and phosphor crystal.

According to the application of Mie theory, calculating C_{sca} can be carried out via:

$$C_{sca} = \frac{2\pi}{k^2} \sum_{0}^{\infty} (2n-1)(|a_n|^2 + |b_n|^2) \quad (8)$$

In this C_{sca} calculation, $k = 2\pi/\lambda$. Meanwhile, parameters a_n and b_n can be attained with below formulas:

$$a_n(x,m) = \frac{\psi_n'(mx)\psi_n(x) - \mathrm{m}\psi_n(mx)\psi_n'(x)}{\psi_n'(mx)\xi_n(x) - \mathrm{m}\psi_n(mx)\xi_n'(x)} \quad (9)$$

$$b_n(x,m) = \frac{m\psi_n'(mx)\psi_n(x) - \psi_n(mx)\psi_n'(x)}{m\psi_n'(mx)\xi_n(x) - \psi_n(mx)\xi_n'(x)} \quad (10)$$

Here, $x = k.r$, m is the refractive index, while $\psi_n(x)$ and $\xi_n(x)$ are the Riccati-Bessel function.

Accordingly, the relative refractive indices of diffusor and phosphor, indicated by m_{dif} and m_{phos}, respectively, in the silicone are possibly obtained via: $m_{dif} = n_{dif}/n_{sil}$ and $m_{phos} = n_{phos}/n_{sil}$, and the phase function is calculated by:

$$p(\theta,\lambda,r) = \frac{4\pi\beta(\theta,\lambda,r)}{k^2 C_{sca}(\lambda,r)} \quad (11)$$

where $\beta(\theta, \lambda, r)$, $S_1(\theta)$ and $S_2(\theta)$ are the angular scattering amplitudes obtained from these equations:

$$\beta(\theta,\lambda,r)=\frac{1}{2}[|S_1(\theta)|^2+|S_2(\theta)|^2] \quad (12)$$

$$S_1=\sum_{n=1}^{\infty}\frac{2n+1}{n(n+1)}\begin{bmatrix}a_n(x,m)\pi_n(\cos\theta)\\ +b_n(x,m)\tau_n(\cos\theta)\end{bmatrix} \quad (13)$$

$$S_2=\sum_{n=1}^{\infty}\frac{2n+1}{n(n+1)}\begin{bmatrix}a_n(x,m)\tau_n(\cos\theta)\\ +b_n(x,m)\pi_n(\cos\theta)\end{bmatrix} \quad (14)$$

3. RESULTS AND DISCUSSION

Figure 2 illustrates the lumen output influenced by the concentration of SiO_2 in the LED package. When the concentration of SiO_2 in the experimented model is 1%, the photoluminescence is 12% greater than that of the conventional structure with the same concentration for the yellow phosphor. This result can be explained by the higher amount of yellow lights in the nanoparticles incorporated encapsulant package due to the better conversion of the blue lights from the LED chips. Specifically, SiO_2 scattering ability helps to prolong the blue-light optical path by preventing the Lambertian blue ray from directly going through the silicone encapsulant, resulting in stronger excitation of the yellow phosphor. Then, there are more and more yellow photons generated, and this finally causes the lumen efficiency to increase. Next, the angular CCT deviations of the SiO_2 embedded package are shown in Figure 3. The results were recorded with different SiO_2 concentrations. The CCT uniformity in general can be demonstrated by the subtraction of the maximum and minimum CCT values. When SiO_2 is not blended into the encapsulation layer, the CCT deviation is high (approximately 5,319 K), implying the high volume of extracted blue lights. Meanwhile, with SiO_2 in the encapsulant, the CCT variations between 0^0 and 70^0 seems to be eliminated, owing to the higher ratio of yellow conversion caused by the strong scattering effect of SiO_2 layer. Moreover, as the concentration of SiO_2 increases to 10%, the CCT deviation significantly declines to 7 K while it is 522 K when the concentration of SiO_2 is 0%.

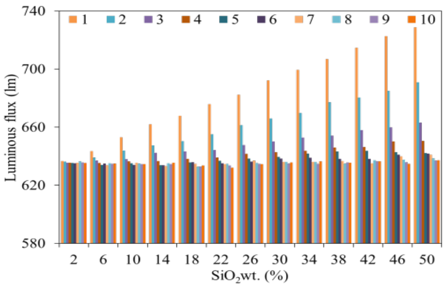

Figure 2. Luminous fluxes of SiO_2 particles with different diameters

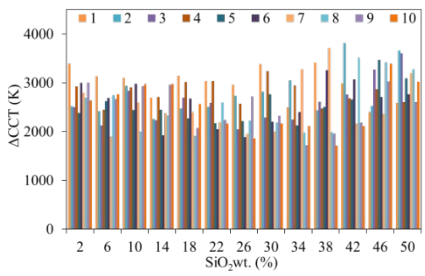

Figure 3. CCT deviations of SiO_2 particles with different diameters

To further analyze the characteristics of SiO_2-doped layer in WLEDs, we conducted experiments on the SiO_2-phosphor-silicone encapsulation layer, and these experiments include transmission-absorption and haze. The results shows that the absorption of SiO_2-doped structure is higher than that of the non-SiO_2 one, which increased from around 32% to approximately 42% at the wavelength of 460 nm, see Figure 4 and Figure 5. Then, this increase generates more yellow light portions in the SiO_2-integrated layer, leading to higher lumen efficacy. In these experiments, the change in concentration greatly impacts the effect of SiO_2-incorporated sample, which can be demonstrated through the refractive index (RI) of the layer. The RI equation of the encapsulation layer comprised of silicone, phosphor, and SiO_2 nanoparticles is as follow:

$$RI = V_1RI_1 + V_2RI_2 + V_3RI_3 \quad (15)$$

In which V_1, V_2 and V_3 indicate the material concentrations, which are determined by the weight percentages of the materials. Noted that the refractive indexes of silicone, phosphor, and SiO_2 nanoparticles are 1.4, 1.8 and 2.23, in turn, at the wavelength of 460 nm. The size of SiO_2 nanoparticles is 300 nm. The concentrations of SiO_2 nanoparticle mixed into the phosphor-silicone film are 1 wt% and 3 wt%, respectively. After calculating, the RIs of the encapsulation layer with each SiO_2 concentration are 1.428 and 1.445.

In addition, the TFCalc32 simulation is applied to determine the effect of these layers. Different from the traditional structure, the light extractions of these two SiO_2-doped designs are nearly equal to each other because the difference between the refractive index of 1% SiO_2 layer and that of 3% SiO_2 one is very small. Therefore, it can be concluded that the only factor that affects the improvement of lumen output is the SiO_2 scattering effect which can be evaluated by applying the Mie-scattering theory. Moreover, the experimented results present that structure with lower concentration of SiO_2 exhibits the haze intensity of approximately 100% before reaching the wavelength of 500 nm. However, when the wavelength is longer than 50 nm, this value tends to decline slowly. Besides that, when the concentration of SiO_2 increases, the values of haze intensity are relatively the same in the wavelength range of 300-700 nm, see Figure 6 and Figure 7.

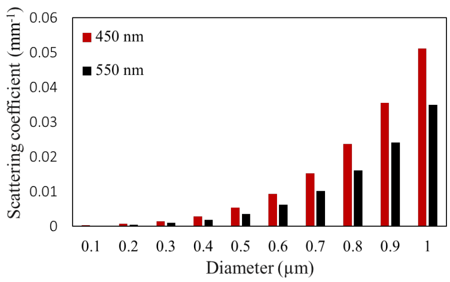

Figure 4. Scattering coefficients of SiO_2 particles at 450 and 550 nm

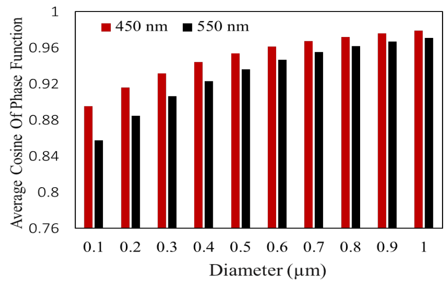

Figure 5. The phase function of SiO_2 particles at 450 and 550 nm

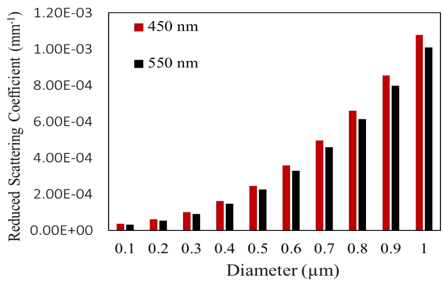

Figure 6. The reduced scattering coefficient of SiO_2 particles at 450 and 550 nm

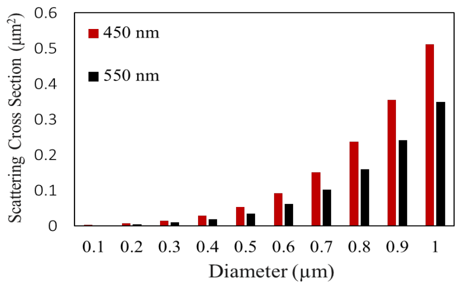

Figure 7. The scattering cross section of SiO_2 particles at 450 and 550 nm

4. CONCLUSION

In summary, this study demonstrated the influence of SiO_2 on the lighting performances of WLEDs when being integrated into the phosphor-silicone encapsulation layer. The results indicate that the luminous efficiency can be 12% better when 1% SiO_2 is added. The enhancement in lumen output is attributed to the strong scattering effect of SiO_2 and the improvement in the blue-light utilization. The CCT uniformity of WLED devices is also benefited from SiO_2 content. With 10% SiO_2 in the encapsulation layer, the CCT deviation drop to 7 K from 522 K. Especially, this SiO_2-doped design do not cause any considerable disadvantage to the lumen output as the SiO_2 concentration increases. According the result from the haze computations, the haze intensity is in direct proportion to the concentration of doped SiO_2. In other words, haze intensity can reach 100% if the content of SiO_2 nanoparticles keep increasing. Thus, SiO_2 nanoparticles can be a great solution to simultaneously enhance angular CCT homogeneity and luminous flux of WLED devices.

REFERENCES

[1] A. K. Dubey, M. Gupta, V. Kumar, and D. S. Mehta, "Laser-line-driven phosphor-converted extended white light source with uniform illumination," *Appl. Opt.*, vol. 58, no. 9, pp. 2402-2407, 2019, doi: 10.1364/AO.58.002402.

[2] C. Zhang, *et al.*, "Exciton photoluminescence of $CsPbBr_3$@SiO_2 quantum dots and its application as a phosphor material in light-emitting devices," *Opt. Mater. Express,* vol. 10, no. 4, pp. 1007-1017, 2020, doi: 10.1364/OME.389847.

[3] X. Wang, Y. Wang, J. Yu, Y. Bu, and X. Yan, "Modifying phase, shape and optical thermometry of $NaGdF_4$:2%Er^{3+} phosphors through Ca^{2+} doping," *Opt. Express,* vol. 26, no. 17, pp. 21950-21959, 2018, doi: 10.1364/OE.26.021950.

[4] B. Qiu, K. Li, and X. Li "Synthesis and enhanced luminescent properties of SiO2@LaPO4:Ce3+/Tb3+ microspheres," *Opt. Mater. Express,* vol. 8, no. 1, pp. 59-65, 2018, doi: 10.1364/OME.8.000059.
[5] N. Q. Li, *et al.*, "High-efficiency solution-processed WOLEDs with very high color rendering index based on a macrospirocyclic oligomer matrix host," *Opt. Mater. Express,* vol. 8, pp. 3208-3219, 2018, doi: 10.1364/OME.8.003208.
[6] Z. Huang, Q. Liu, M. R. Pointer, W. Chen, Y. Liu, and Y. Wang "Color quality evaluation of Chinese bronzeware in typical museum lighting," *J. Opt. Soc. Am. A,* vol. 37, no. 4, pp. A170-A180, 2020, doi: 10.1364/JOSAA.381498.
[7] Y. Yu, *et al.*, "Improving the color-rendering index of a tandem warm white organic light-emitting device by employing a simple fabrication process," *Opt. Lett*, vol. 44, no. 4, pp. 931-934, 2019, doi: 10.1364/OL.44.000931.
[8] S. J. Dain, D. A. Atchison, J. K. Hovis, and M.-Y. Boon, "Lighting for color vision examination in the era of LEDs: the FM100Hue Test," *J. Opt. Soc. Am. A,* vol. 37, no. 4, pp. A122-A132, 2020, doi: 10.1364/JOSAA.382301.
[9] X. Hu, *et al.,* "Optimizing selection of the test color sample set for the CIE 2017 color fidelity index," *Opt. Express,* vol. 28, no. 6, pp. 8407-8422, 2020, doi: 10.1364/OE.383283.
[10] S. Song, *et al.,* "Tailoring active color rendering and multiband photodetection in a vanadium-dioxide-based metamaterial absorber," *Photon. Res*, vol. 6, no. 6, pp. 492-497, 2018, doi: 10.1364/PRJ.6.000492.
[11] H. Chen, *et al.,* "Quadrichromatic LED based mobile phone camera visible light communication," *Opt. Express,* vol. 26, no. 13, pp. 17132-17144, 2018, doi: 10.1364/OE.26.017132.
[12] H. Lee, *et al.,* "Color-tunable organic light-emitting diodes with vertically stacked blue, green, and red colors for lighting and display applications," *Opt. Express,* vol. 26, no. 14, pp. 18351-18361, 2018, doi: 10.1364/OE.26.018351.
[13] T. Wu, *et al.,* "Analyses of multi-color plant-growth light sources in achieving maximum photosynthesis efficiencies with enhanced color qualities," *Opt. Express,* vol. 26, no. 4, pp. 4135-4147, 2018, doi: 10.1364/OE.26.004135.
[14] P. Zhu, H. Zhu, G. C. Adhikari, and S. Thapa, "Design of circadian white light-emitting diodes with tunable color temperature and nearly perfect color rendition," *OSA Continuum,* vol. 2, no. 8, pp. 2413-2427, 2019, doi: 10.1364/OSAC.2.002413.
[15] X. Liu, *et al.,* "Laser-based white-light source for high-speed underwater wireless optical communication and high-efficiency underwater solid-state lighting," *Opt. Express,* vol. 26, no. 15, pp. 19259-19274, 2018, doi: 10.1364/OE.26.019259.
[16] L. Xu, B. Zhao, and M. R. Luo, "Color gamut mapping between small and large color gamuts: part II. gamut extension," *Opt. Express,* vol. 26, no. 13, pp. 17335-17349, 2018, doi: 10.1364/OE.26.017335.
[17] S. Pan, B. Yang, X. Xie, and Z. Yun, "Image restoration and color fusion of digital microscopes," *Appl. Opt*, vol. 58, no. 9, pp. 2183-2189, 2019, doi: 10.1364/AO.58.002183.
[18] Q. Song, *et al.,* "Vicarious calibration of COCTS-HY1C at visible and near-infrared bands for ocean color application," *Opt. Express,* vol. 27, no. 20, pp. A1615-A1626, 2019, doi: 10.1364/OE.27.0A1615.
[19] P. J. Pardo, M. I. Suero, and Á. L. Pérez, "Correlation between perception of color, shadows, and surface textures and the realism of a scene in virtual reality," *J. Opt. Soc. Am. A,* vol. 35, no. 4, pp. B130-B135, 2018, doi: 10.1364/JOSAA.35.00B130.
[20] Y. L. Piao, M.-U. Erdenebat, K.-C. Kwon, S.-K. Gil, and N. Kim, "Chromatic-dispersion-corrected full-color holographic display using directional-view image scaling method," *Appl. Opt*, vol. 58, no. 5, pp. A120-A127, 2019, doi: 10.1364/AO.58.00A120.
[21] C. Bai, *et al.,* "Full-color optically-sectioned imaging by wide-field microscopy via deep-learning," *Biomed. Opt. Express,* vol. 11, no. 5, pp. 2619-2632, 2020, doi: 10.1364/BOE.389852.
[22] O. Kunieda, and K. Matsushima, "High-quality full-parallax full-color three-dimensional image reconstructed by stacking large-scale computer-generated volume holograms," *Appl. Opt*, vol. 58, no. 34, pp. G104-G111, 2019, doi: 10.1364/AO.58.00G104.
[23] K. Matsushima, and N. Sonobe, "Full-color digitized holography for large-scale holographic 3D imaging of physical and nonphysical objects," *Appl. Opt*, vol. 57, no. 1, pp. A150-A156, 2018, doi: 10.1364/AO.57.00A150.
[24] F. Guan, G. Jiang, Y. Song, M. Yu, Z. Peng, and F. Chen, "No-reference high-dynamic-range image quality assessment based on tensor decomposition and manifold learning," *Appl. Opt*, vol. 57, no. 4, pp. 839-848, 2018, doi: 10.1364/AO.57.000839.
[25] R. E. O'Shea, S. R. Laney, and Z. Lee., "Evaluation of glint correction approaches for fine-scale ocean color measurements by lightweight hyperspectral imaging spectrometers," *Appl. Opt*, vol. 59, no. 7, pp. B18-B34, 2020, doi: 10.1364/AO.377059.
[26] J. J. Gómez-Valverde, *et al.,* "Automatic glaucoma classification using color fundus images based on convolutional neural networks and transfer learning," *Biomed. Opt. Express,* vol. 10, no. 2, pp. 892-913, 2019, doi: 10.1364/BOE.10.000892.
[27] A. Neitz, *et al.,* "Effect of cone spectral topography on chromatic detection sensitivity," *J. Opt. Soc. Am. A,* vol. 37, no. 4, pp. A244-A254, 2020, doi: 10.1364/JOSAA.382384.